Structural Engineering and Mechanics, *Vol. 65, No. 5 (2018) 633-644*
DOI: https://doi.org/10.12989/sem.2018.65.5.633

Component fragility assessment of a long, curved multi-frame bridge: Uniform excitation versus spatially correlated ground motions

Jong-Su Jeon*[1], Abdollah Shafieezadeh[2a] and Reginald DesRoches[3b]

[1]*Department of Civil Engineering, Andong National University, 1375 Gyeongdong-ro, Gyeongsangbuk-do 36729, Republic of Korea*
[2]*Department of Civil, Environmental and Geodetic Engineering, The Ohio State University, 2070 Neil Ave., Columbus, OH 43210, USA*
[3]*Department of Civil and Environmental Engineering, Rice University, 6100 Main Street, Houston, TX 77005, USA*

(Received October 24, 2017, Revised January 2, 2018, Accepted January 3, 2018)

Abstract. This paper presents the results of an assessment of the seismic fragility of a long, curved multi-frame bridge under multi-support earthquake excitations. To achieve this aim, the numerical model of columns retrofitted with elliptical steel jackets was developed and validated using existing experimental results. A detailed nonlinear numerical model of the bridge that can capture the inelastic response of various components was then created. Using nonlinear time-history analyses for a set of stochastically generated spatially variable ground motions, component demands were derived and then convolved with new capacity-based limit state models to obtain seismic fragility curves. The comparison of failure probabilities obtained from uniform and multi-support excitation analyses revealed that the consideration of spatial variability significantly reduced the median value of fragility curves for most components except for the abutments. This observation indicates that the assumption of uniform motions may considerably underestimate seismic demands. Moreover, the spatial correlation of ground motions resulted in reduced dispersion of demand models that consequently decreased the dispersion of fragility curves for all components. Therefore, the spatial variability of ground motions needs to be considered for reliable assessment of the seismic performance of long multi-frame bridge structures.

Keywords: long, curved multi-frame bridge; nonlinear numerical bridge model; spatially variable ground motions; multi-support excitation analysis; component fragility curves

1. Introduction

During earthquakes, ground motions that excite multiple supports of large structures such as dams, pipelines, and bridges may differ significantly. Thus, realistic seismic assessment of these structures must account for the spatial variation of ground motions over the entire length of such a structure. In other words, input motions that are imposed at the supports not only should possess realistic characteristics individually, but also should be properly correlated with each other. Nevertheless, current seismic design codes and methods of practice and risk assessment do not properly account for the effect of spatially variable ground motions on the response of large, geographically distributed structures such as multi-frame bridges. Spatial variation in ground motion characteristics in the time and frequency domains may cause damage to structures. For instance, Moehle (1994) reported that the partial collapse of two connectors that are located far from each other among the four multi-frame bridges and numerous shorter bridges on the Interstate 5/Route 14 interchange that occurred during the 1994 Northridge earthquake was caused by the large spatial variation of ground motions. Accordingly, several analytical studies have investigated multi-support excitations and their impacts on the seismic performance of geographically distributed structures. The focus of these studies was: (1) development of procedures for simulating spatially correlated ground motions through stochastic random processes (Vanmarcke and Fenton 1991, Vanmarcke *et al.* 1993, Der Kiureghian 1996, Shinozuka *et al.* 2000, Hu *et al.* 2006, Liao and Zerva 2006, Konakli and Der Kiureghian 2011), and (2) derivation of fragility curves using different support motions simulated by stochastic methods (Deodatis *et al.* 2000, Kim and Feng 2003, Peña Ramos and Haldar 2012). Der Kiureghian (1996) indicated that spatial variability in strong ground motions can significantly affect the internal forces induced in structures, such as bridges and viaducts, which are characterized by multiple supports. Variability in the support motions usually tends to reduce the inertia-generated forces within the structures. However, different support motions generate additional forces, known as pseudo-static forces, that are absent when the structure is subjected to uniform support motions (Der Kiureghian 1996). Additionally, Shinozuka *et al.* (2000) and Kim and Feng (2003) showed that multiple support motions triggered at different locations within multi-frame bridges produce significantly higher structural responses than do uniform support motions. This finding demonstrates that maximum deformation demands in columns are underestimated if uniform support motions are presumed, resulting in lower exceedance probabilities of observed damage states.

*Corresponding author, Assistant Professor
E-mail: jsjeon@anu.ac.kr
[a]Assistant Professor
[b]Professor

ISSN: 1225-4568 (Print), 1598-6217 (Online)

Stochastic random processes for the simulation of spatially variable ground motions have been performed in two categories: (1) unconditional simulations that use only user-prescribed space-time statistics to generate inter-correlated motions that are not conditioned on any recorded motion (Der Kiureghian 1996, Deodatis *et al.* 2000, Shinozuka *et al.* 2000, Kim and Feng 2003, Konakli and Der Kiureghian 2011, Peña Ramos and Haldar 2012), and (2) conditional simulations generating correlated ground motions that are statistically compatible with or are conditioned on recorded ground motions at nearby points (Vanmarcke and Fenton 1991, Vanmarcke *et al.* 1993, Liao and Zerva 2006, Hu *et al.* 2012). Because the unconditional simulation provides a valuable tool for evaluating the seismic responses of structures, recent studies (Deodatis *et al.* 2000, Shinozuka *et al.* 2000, Kim and Feng 2003, Peña Ramos and Haldar 2012) have employed unconditional stochastic random processes to develop the fragility curves of multi-frame bridges. However, a conditional stochastic random process has yet to be used for the generation of these fragility curves. The method of unconditional ground motion simulation has the shortcoming that simulated motions possess limited association with actual seismic records (Liao and Zerva 2006). This drawback can be alleviated through conditional stochastic process that can simulate ground motions compatible with prescribed ground motions whether actual recorded data or synthetic ground motions. Additionally, Liao and Zerva (2006) stated that the motions obtained from the conditional simulation process possess physical characteristics of the prescribed motions such as non-stationarity in amplitude and frequency content as well as the effects of earthquake magnitude, source-site distance, and local soil conditions, among other features. Thus, this study employed the conditional stochastic random process to perform the probabilistic seismic assessment of bridges.

This study focused on assessing the seismic vulnerability of a long, curved, multi-frame concrete box-girder bridge that experienced different support motions. A conditional stochastic random process was used to simulate multi-support motions that were conditioned on a set of ground motions recorded at a specific site. A detailed numerical model of the bridge was created using OpenSees (McKenna 2011). NTHAs for the bridge under both uniform and multi-support motions were performed. Using results of a set of NTHAs, component demand models were developed and convolved with limit state models to generate component fragility curves. Finally, these component fragilities obtained from uniform and multi-support excitation analyses were compared to investigate the effect of spatially correlated ground motions on the seismic reliability of components.

2. Numerical bride model and model validation

This section provides a description of the bridge and details of various bridge component models. In particular, it presents the model validation of an elliptical steel-jacketed column, which is one of the most critical components in the subject bridge system.

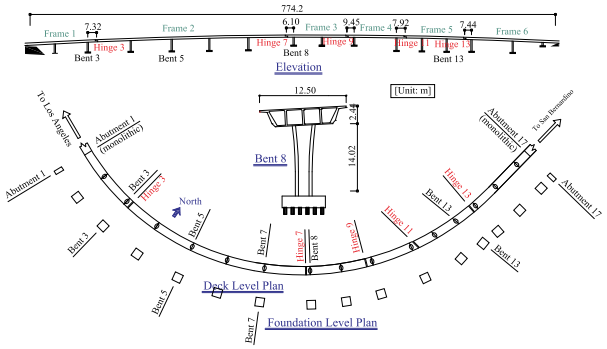

Fig. 1 Plan, elevation, and sensor location of the Northwest Connector

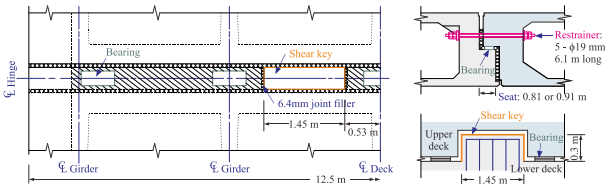

Fig. 2 Details of the in-span hinges

2.1 Description of subject bridge

The bridge examined in this study is the Northwest Connector, which is located at a freeway interchange in Colton, California that links the east-west I10 freeway with the north-south I215 freeway about 85 km east of downtown Los Angeles. The plan and elevation of the Northwest Connector are depicted in Fig. 1. This bridge was seismically strengthened by the California Department of Transportation in 1991 due to the significance of the traffic operation of the two Interstate routes and their location within the San Jacinto fault zone (Fenves and DesRoches 1994). After this rehabilitation, the bridge was struck by the 1992 Landers and Big Bear earthquakes. Additionally, Jackura *et al.* (1991) indicated that the downhole tests at the bridge site provided an estimate of 480 m/sec for the average shear wave for alluvial sands.

The subject bridge is a curved concrete box-girder bridge that is 774 m long with 16 spans supported by 15 single column bents and two diaphragm abutments. Beginning at Abutment 1, the alignment has 310 m and 386 m lengths on 366 m and 396 m radius curves, respectively, and a 77 m straight segment ending at Abutment 17 (Fig. 1). The overall bridge system is composed of six frames connected at five in-span hinges (Hinges 3, 7, 9, 11, and 13). These frames have a reinforced and prestressed box-girder superstructure of 12.5 m in width and 2.45 m in depth supported by two to four single column bents. The original columns have a 2.44 m by 1.68 m octagonal section, while the retrofitted columns have an elliptical cross-section with overall dimensions of 2.69 m by 2.06 m. For the retrofitted columns, a 13 mm thick steel casing in an elliptical shape was used to improve the confinement, shear strength, and flexural ductility of the columns. Two types of column retrofits were employed: full-height steel jackets were used to encase the columns at 12 of the 15 bents, and partial-height steel jackets were used for three of the 15

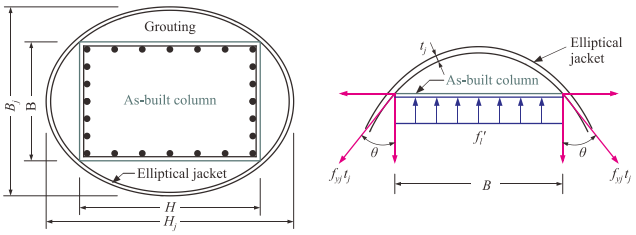

Fig. 3 Cross-section and equivalent confining stress of elliptical steel-jacketed column

bents (Bents 8, 12, and 14). The partial-height steel jackets extended only over the lower 5.49 m of the columns. Diaphragm abutments with 4.0 m high backwalls and 5.5 m long tapered wing walls are integral with the box girder. The columns and abutments have pile foundations (concrete and steel tube piles for original and retrofitted pile caps, respectively). As illustrated in Fig. 2, the five in-span hinges have a seat width of 0.91 m (for Hinges 3 and 7) or 0.81 m (for Hinges 9, 11, and 13). The hinge support is provided by elastomeric bearing pads of thickness ranging from 102 mm to 140 mm. A 1.45 m long and 0.30 m deep shear key exists to prevent relative tangential displacement at the hinges. The sides of the shear key have 6.4 mm of joint filler. In addition, the original restrainers that consisted of four cable units across all of the five hinges were replaced with longer cable restrainers to prevent excessive relative displacements that could lead to unseating. Each new cable unit is 6.1 m in length and is composed of five 19 mm diameter twisted strand cables. As a result, these hinges allow relative radial displacement by the restrainers and bearings, but restrain relative tangential displacement by the shear keys.

2.2 Model of elliptical steel-jacketed columns

2.2.1 Numerical column model

Columns are generally recognized as the most critical of components in a bridge system, being essential components that can affect the global collapse of a bridge (lateral and axial load carrying capacity). To capture the nonlinear response of columns (here, elliptical steel-jacketed columns), a numerical flexure response model was built using OpenSees (McKenna 2011). Each column was modeled using six fiber-type displacement-based, beam-column elements. In the fiber sections, the *Hysteretic* material model was used to simulate the longitudinal reinforcement with a hardening factor of 0.01 and the *Concrete02* material model was used to include the tensile behavior of unconfined and confined concrete. The confined concrete was simulated using the model reported by Mander *et al.* (1988) with modification to the confining pressure associated with an elliptical steel jacket as proposed by Priestley *et al.* (1994a).

The elliptical cross-section and the equivalent confining stress induced by the steel casing of a retrofitted column are illustrated in Fig. 3. Considering a unit length of a rectangular column that is transversely confined by an elliptical jacket, the equivalent confining stress (f_l') in the strong and weak directions at the jacket yielding can be

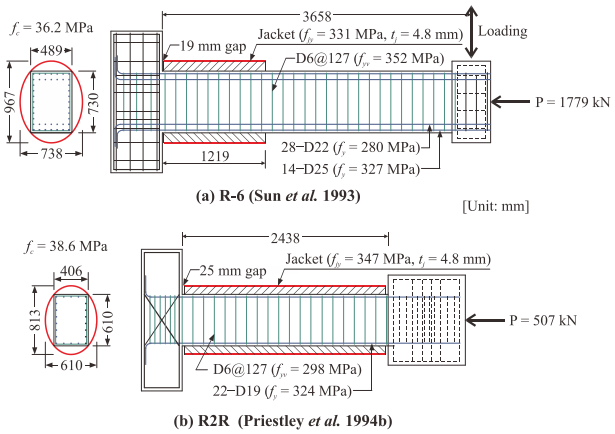

Fig. 4 Details of elliptical steel-jacketed columns

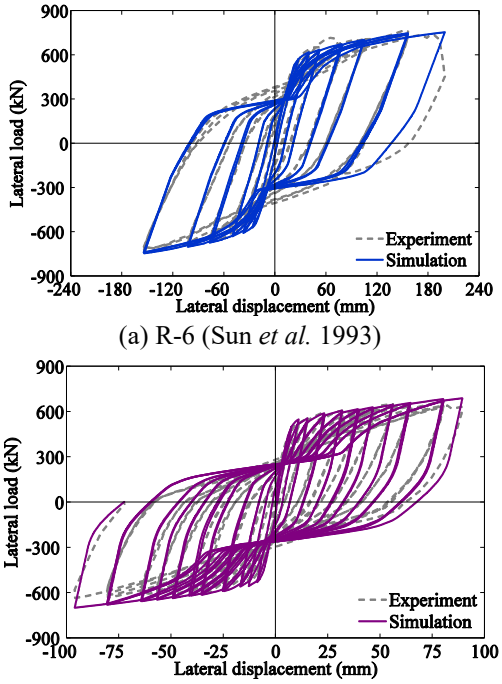

(a) R-6 (Sun *et al.* 1993)

(b) R2R (Priestley *et al.* 1994b)

Fig. 5 Observed and simulated responses for elliptical steel-jacketed columns

expressed as

$$f_l' = \begin{cases} \dfrac{2 f_{jy} t_j \cos(\theta)}{B}; & \text{in the strong direction} \\ \dfrac{2 f_{jy} t_j \cos(\theta)}{H}; & \text{in the weak direction} \end{cases} \quad (1)$$

where

$$\theta = \begin{cases} \tan^{-1}\left(\dfrac{B_j H}{H_j \sqrt{H_j^2 - H^2}} \right); & \text{in the strong direction} \\ \tan^{-1}\left(\dfrac{H_j B}{B_j \sqrt{B_j^2 - B^2}} \right); & \text{in the weak direction} \end{cases} \quad (2)$$

and f_{yj} and t_j are the yield strength and thickness of the steel jacket, respectively. B and H are the corresponding section dimensions of the original rectangular column while B_j and H_j are the section dimensions of the elliptical steel-jacketed column. θ is the tangential angle of the jacket at the corner of the column section in the strong and weak directions. The average confining stress (f_l') is used to determine key parameters of the steel-jacket confined concrete model.

2.2.2 Model validation

The ability of the above column model to capture inelastic responses was examined by comparing the results of experimental simulations with data from previous studies. In this study, two specimens were selected: one being the partial-height steel-jacketed columns tested by Sun *et al.* (1993) for enhancement of the flexural strength and ductility of columns, and one being the full-height steel-jacketed columns tested by Priestley *et al.* (1994b) for improvement of the shear strength of columns. Fig. 4 shows the test configuration, cross-section, reinforcing details, and material properties for the two retrofitted columns. These specimens were subjected to lateral loadings only in the strong direction because of an insufficient number of column tests under cyclic loadings in the weak direction. Results indicate that the simulated responses agree very well with observed responses for all of the specimens with regard to stiffness, strength, and energy dissipation (Fig. 5).

2.2.3 Bridge system model

The numerical model of the Northwest Connector created using OpenSees (McKenna 2011) is outlined in Fig. 6. Since it was expected that the deck would remain elastic during earthquakes, the superstructure of the bridge was modeled as a spine with elastic beam-column elements at the elastic centroid of the members along the bridge length. The effective flexural stiffness for reinforced and prestressed box girders was computed based on 75% (cracked) and 100% (uncracked) of gross stiffness, respectively, following the recommendation of Buckle *et al.* (2006). The flexural stiffness for deck elements near piers (where a moment transfer exists between the superstructure and pier) was reduced to account for the shear lag effect.

The effective deck width was taken as the column width at the top plus two times the depth of the deck (Priestley *et al.* 1996, Caltrans 2013) within one-quarter of the span of each bent. The torsional rigidity for a cellular superstructure was computed using the rational shear flow theory (Priestley *et al.* 1996). To represent the diaphragms and in-span hinges and to capture the torsion of the box girder due to the bridge curvature, the transverse beam elements were modeled using elastic beam-column elements (rigid and massless). Because of light traffic at the time of two earthquakes (1992 Landers and Big Bear earthquakes), the mass of the superstructure accounted only for the dead loads. The translational mass was lumped at the nodes of the longitudinal superstructure elements. The torsional mass of inertia about the bridge alignment axis was included to reflect the effect of twisting (Buckle *et al.* 2006). To achieve this goal, the torsional mass of inertia (I_T) for the cross-section of the box girder was converted into vertical masses by dividing it by the superstructure width (b_s). The

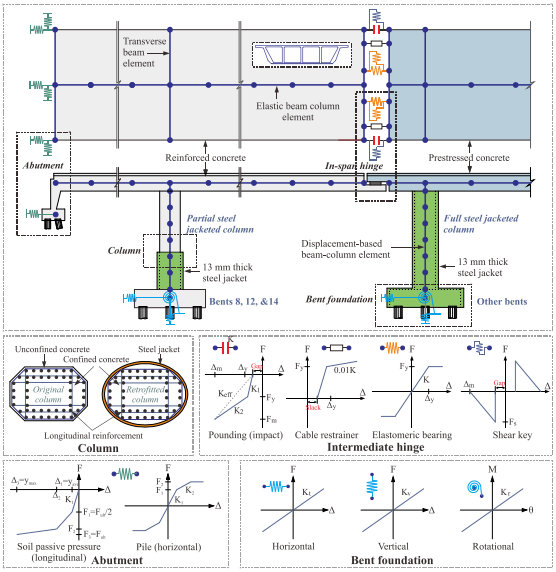

Fig. 6 Illustration of the numerical bridge model and its component models

vertical lumped mass at the end of the transverse beam element was $I_T/(2b_s)$, and the remaining mass was lumped at the centerline along the bridge alignment axis (Jeon *et al.* 2016). In this study, the vertical mass lumped at the end node was approximately 40% of the total vertical mass.

As shown in Fig. 2, an in-span hinge is comprised of both explicit components (such as cable restrainers, elastomeric bearings, and a shear key) as well as implicit components (such as pounding between adjacent decks). To capture this composite behavior in in-span hinges, an in-span hinge model was developed by combining component response models (Fig. 6). The implicit component (pounding) was modeled using a nonlinear compression element with the gap being modeled as proposed by Muthukumar and DesRoches (2006). The first and second negative stiffnesses of the pounding element were found to be 10,680 kN/mm and 3680 kN/mm, respectively. A gap distance of 38 mm was assigned to all in-span hinges. The cable restrainer was modeled using a bilinear tension-only element with an initial level of slackness and a hardening factor of 0.01 (Fig. 6) (Caltrans 2017). The stiffness and yield force per cable were assumed to be 8 kN/mm and 174 kN, respectively. The initial slack measurements were 13 mm for Hinges 3 and 7, and 25 mm for Hinges 9, 11, and 13. In addition, the nonlinear response of elastomeric bearings was simulated using an elastic perfectly plastic model with shear modulus of 1.0 MPa. The initial stiffness was calculated as the product of the shear modulus and the pad area divided by the bearing height. The size of bearing pads (width × depth × height) was 711 mm × 305 mm × 140 mm for Hinges 3 and 7, 406 mm × 356 mm × 76 mm for Hinges 9 and 11, and 508 × 356 × 102 mm for Hinge 13. The yield force was calculated by multiplying the normal force acting on the bearing with the coefficient of friction of the pad (f_b = 0.4) recommended by Caltrans (2013). The nonlinear response of shear keys in the in-span hinge model was simulated on the basis of experimental results by Megally *et al.* (2002), as shown in Fig. 6. The

maximum shear key force was defined as the minimum of design forces obtained from four different failure mechanisms such as shear friction, flexure, shear, and bearing. The size of shear keys (length × depth × height) is 1450 mm × 813 mm × 305 mm, and the gap between the shear key and the upper deck is 6.4 mm. In accordance with the experimental observation by Megally *et al.* (2002), the maximum displacement was the gap plus 90 mm and the corresponding force was zero. Moreover, the relative vertical displacement and twisting at the in-span hinge were constrained to be zero.

Columns were modeled as presented in the previous section using fiber-type displacement-based beam-column elements along with rigid links at the superstructure-column and footing-column connections. Since all columns were retrofitted by the steel jacket, the shear capacity of the columns would be significantly improved, and thus shear response model were not included. The mass was lumped at the nodes of the column elements. The pile foundations were modeled using lumped linear springs. The stiffnesses were computed using the relationships presented in Ma and Deng (2000). The formulation of the springs accounts for geometry and pile group effects. These springs include two translational springs, one vertical spring, and two rotational springs. The effective translational and vertical stiffnesses were calculated assuming a stiffness of 7 kN/mm/pile (Caltrans 2013) and 175 kN/mm/pile (Choi *et al.* 2004), respectively. The effective rotational stiffnesses for a pile group were estimated using the geometry of the piles and the vertical stiffness of an individual pile. In addition, the translational and rotational mass of the pile caps were lumped at the footing-column connection.

Lumped nonlinear translational springs were employed at the level of the abutment backwall to capture the inelastic response of the abutments in the radial and tangential directions. The longitudinal response consisted of active (tensile) and passive (compressive) actions. The passive and active resistances were assumed to provide the composite action of soil and piles, and piles alone, respectively. The transverse response of the abutment was assumed to be resisted only by the piles. To simulate the abutment backwall soil in the passive action, the hyperbolic soil model of developed by Shamsabadi *et al.* (2010) was employed with modification to a trilinear spring model for computational efficiency. This modification was achieved by using the equal-area rule for the hyperbolic backbone curve. The computed initial stiffness and ultimate passive resistance of the soil were 390 kN/mm and 547 kN, respectively. The pile response was simulated by the trilinear spring model proposed by Choi *et al.* (2004) using a translational stiffness of 7 kN/mm per pile.

3. Conditional simulation of spatially correlated Ground motions

This study follows the approach proposed by Vanmarcke *et al.* (1993) to simulate different unknown support motions through conditional simulation and a known ground motion at a bridge support. The detailed description of this approach can be found in the reference.

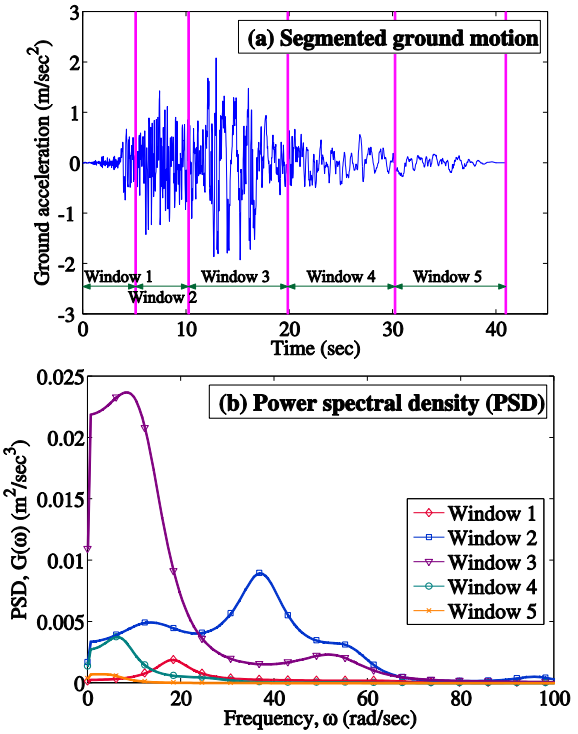

Fig. 7 Segmented motions and associated PSDs for a known earthquake accelerogram

This section explains key characteristics of the conditional simulation method used in this study. To simulate non-stationary motions (more realistic ground motions) in which both the frequency content and amplitude evolve with time, the known acceleration time history was divided into m segments with different spectral densities, as shown in Fig. 7(a), each of which was considered stationary. The range of each segmented motion was determined based on the amplitude, frequency, and envelope of vibrations. Each power spectral density function (PSD) was estimated in the consecutive time windows, as depicted in Fig. 7(b), using the Burg method (Burg 1972, Bos *et al.* 2002). This approach fits an autoregressive model to the signal by minimizing forward and backward prediction errors in the least-squares sense. Each PSD was used to simulate the corresponding stationary segment of the motion, and a non-stationary time history was achieved by piecing the simulated stationary segments together via the linear interpolation algorithm developed by Vanmarcke *et al.* (1993).

Another critical feature is to define the coherency model between known and unknown ground motions. This study adopts the empirical coherency model, $\rho(\omega,r)$, suggested by Luco and Wong (1986), which is one of the most widely used models (Liao and Zerva 2006)

$$\rho(\omega,r)=\exp\left(-\alpha^2\omega^2r^2\right) \tag{3}$$

where r is the separation distance between points x_i and x_j (m), ω is the frequency (rad/sec), and α is the coherency drop parameter (sec/m). Luco and Wong (1986) recommended a α of 2×10^{-4}~3×10^{-4} sec/m. Additionally, Konakli and Der Kiureghian (2011) showed that larger

values of α ranging from 3×10^{-4} to 11×10^{-4} sec/m) provide a fairly good approximation for the US Geological Survey Parkfield Seismograph Array recordings (recorded during the 2004 Parkfield earthquake) than the recommended values above. These values will be used in the generation of ground motions in Section 4.3.2.

The algorithm developed by Vanmarcke *et al.* (1993) separately provides pairs of acceleration or displacement time histories for both input and output motions. If the displacement time histories are available from existing ground motion sets, they can be directly imposed to the supports in the OpenSees model without any additional effort. However, most available ground motion sets (Somerville *et al.* 1997, Baker *et al.* 2011) provide only acceleration time histories, and therefore a procedure for the conversion of accelerations to displacement time histories was required. To do this, this study used the method proposed by Liao and Zerva (2006). This procedure is summarized in the following steps.

(1) Subtract the mean value from the entire acceleration time histories.

(2) Apply a short cosine taper function to the simulated acceleration time histories to set their initial values to zero.

(3) Apply a fourth-order, high-pass Butterworth filter (Butterworth 1930) (which is the filter most commonly used by the Center for Engineering Strong Motion Data (Haddadi *et al.* 2008), the US Geological Survey (2015), and the Pacific Earthquake Engineering Research Center (2015)) to the acceleration time histories. The high-pass Butterworth filter was used to remove some contaminations (similar to noises) that were introduced by the large, low-frequency, randomly simulated Fourier amplitude. Here, the corner frequency (f_{cor}) in the high-pass filter was computed using the equation proposed by Liao and Zerva (2006)

$$f_{cor} = \frac{1}{T_f\left[H_0^2/\left(1-H_0^2\right)\right]^{1/2p}} \tag{4}$$

where T_f is the duration of the simulated acceleration time histories, p is the order of the Butterworth filter (= 4), and H_o is the filter amplitude threshold (= 0.02). This step resulted in at least 98% of the low-frequency components with periods longer than the duration of the generated time history being filtered out.

(4) Integrate the resulting acceleration time histories to obtain respective velocity and displacement time histories.

4. Fragility assessment of bridge components

This study follows the approach proposed by Vanmarcke *et al.* (1993) to simulate different unknown support motions through conditional simulation and a known ground motion at a bridge

4.1 Component fragility modeling

Fragility curves are defined as a conditional statement that provides the likelihood of a structure reaching a specified level of damage for a given level of ground motion intensity. These models have found widespread use in probabilistic seismic risk assessment of bridges. A fragility function is typically computed through the convolution of a demand model, called probabilistic seismic demand model (PSDM), with a capacity-based limit state model. The fragility function for a component can be easily estimated using a closed form under the assumptions that both demand and limit state models follow a lognormal distribution

$$P_f = P\left[D \geq C \mid IM\right] = \Phi\left[\frac{\ln\left(S_D/S_C\right)}{\sqrt{\beta_{D|IM}^2+\beta_C^2}}\right] \tag{5}$$

where D and C are the seismic demand and structural capacity, respectively, S_D and $\beta_{D|IM}$ are the median value and dispersion, respectively, of the seismic demand conditioned on the intensity measure (IM), S_C and β_C are the median value and dispersion, respectively, of the structural capacity, and $\Phi(\bullet)$ is the cumulative normal distribution function.

The PSDM can be defined as a linear regression model of seismic demand (D)-intensity measure (IM) pairs for a component in the logarithmic space such that

$$\ln\left(S_D\right) = \ln\left(a\right) + b\ln\left(IM\right) \tag{6}$$

where a and b are the regression coefficients. Data for the regression model are pairs of *D-IM* obtained from NTHAs. From the regression analysis, the dispersion of the model ($\beta_{D|IM}$) is defined in Eq. (7)

$$\beta_{D|IM} = \sqrt{\frac{1}{N-2}\sum_{i=1}^{N}\left[\ln\left(d_i\right)-\ln\left(S_D\right)\right]^2} \tag{7}$$

where d_i is the ith realization of the demands obtained from simulations and N is the number of simulations.

The fragility curve for individual bridge components of the subject bridge under spatially correlated motions can be obtained by conducting the following tasks.

(1) Generate N statistical samples of the subject bridge. These samples are generated by sampling on significant modeling parameters through the Latin hypercube sampling (LHS) technique.

(2) Select a suite of N ground motions that are representative of the seismic hazard of the region.

(3) Stochastically simulate n support motions associated with n locations of interest for each ground motion.

(4) Perform NTHAs for N bridge model-ground motion pairs to monitor the maximum responses of bridge components.

(5) Generate PSDMs for individual components using linear regressions of *D-IM* pairs in the logarithmic space.

(6) Define capacity-based limit state models on the basis of expert judgment, experimental data, analytical models, or combination thereof.

(7) Develop component fragility curves through the convolution of PSDMs and limit state models, as expressed in Eq. (5).

Table 1 Probability distributions used for bridge component models

Random variables	Units	Probability distribution*
Concrete compressive strength (f_c)	MPa	N(μ = 34.5, COV = 12.5%)
Rebar yield strength (f_y)	MPa	LN(μ = 455, COV = 8%)
Steel jacket yield strength (f_{yj})	MPa	N(μ = 276, COV = 10%)
Shear modulus of bearing pad (G_b)	GPa	U (0.55, 1.86)
Coefficient of friction of bearing bad (f_b)	–	LN(μ = 0.4, COV = 10%)
Damping ratio (ξ)	–	N(μ = 0.045, COV = 27%)

*N = normal distribution, LN = lognormal distribution, and U = uniform distribution. μ and COV are the mean value and coefficient of variation, respectively, of a random variable

4.2 Numerical bridge model accounting for uncertainties

This study accounted for uncertainty in material and structural properties by treating modeling parameters as random variables: (1) material properties such as concrete compressive strength (f_c), rebar yield strength (f_y), steel jacket yield strength (f_{yj}), and shear modulus (G_b) and coefficient of friction of elastomeric bearing pad (f_b) and (2) structural damping (ξ). These parameters are inherently random, and this randomness can be modeled by probabilistic models that are based on experimental results. Table 1 summarizes the probability distributions for each of the above parameters, which were determined based on prior studies (Nielson and DesRoches 2007, Padgett and DesRoches 2008). Using the uncertainty in the modeling parameters listed in Table 1, statistically significant yet nominally identical bridge models were developed by sampling across the range of these parameters using the LHS technique. The LHS technique provides a more efficient sampling scheme to cover the probability space of the random variables than does pure random sampling using naive Monte Carlo simulation (Celik and Ellingwood 2010).

4.3 Numerical bridge model accounting for uncertainties

This section briefly explains the conditional stochastic random process used in this study to simulate different unknown support motions through conditional simulation and a known ground motion at a bridge support. This study treats an existing suite of ground motions available in the literature as a set of known ground motions.

4.3.1 An existing suite of real ground motions

Assembling a suite of ground motions that can appropriately represent the seismic hazard of a site is crucial for developing fragility curves applicable to bridge structures that are spread over a wide geographic area. The ground motion suite must contain a wide range of IMs for the area of interest that have been derived from seismic hazard analysis. To address this issue, this study selected the suite of ground motions used in the work of Shafieezadeh *et al.* (2012). The suite consists of 80 ground motions extracted from the PEER Strong Motion Database by Medina and Krawinkler (2003) along with 20 ground motions pertinent to Los Angeles selected from the SAC project database (Somerville *et al.* 1997). The 80 PEER ground motions have an even selection of recorded time histories from four bins that include combinations of low and high magnitudes as well as large and small epicentral distances. The 20 SAC ground motions have 10 pairs with 2% and 10% probability of exceedance within 50 years. This ground motion suite serves as the known ground motions at a reference source for the generation of spatially variable ground motions at the different supports as indicated in Table 2. In addition, the same suite was used to perform uniform excitation analysis. The reference point selected was the base of Bent 8, which is located at the center of the bridge. The ground motions at the supports in the left and right sides of the bent were conditioned on the ground motion at the reference point.

Table 2 Distance (r) from a reference point (Bent 8) to other points

Location	r (m)	Location	r (m)	Location	r (m)
Abutment 1	379	Bent 7	69	Bent 14	268
Bent 2	342	Bent 9	47	Bent 15	307
Bent 3	296	Bent 10	95	Bent 16	351
Bent 4	241	Bent 11	157	Abutment 17	372
Bent 5	181	Bent 12	195		
Bent 6	126	Bent 13	232		

4.3.2 Spatially varying ground motions

Following the procedure proposed by Vanmarcke *et al.* (1993) that is described in Section 3, unknown ground motions at the location of bridge bents were stochastically generated by conditioning them on the prescribed motions. Because the coherency drop parameter (α) is a major source of uncertainty on the simulation of spatially varying ground motions, this study regarded this parameter as a random variable with a uniform distribution in (2×10^{-4}, 11×10^{-4} sec/m). The lower and upper bounds are determined per Luco and Wong (1986) and Konakli and Der Kiureghian (2011). Each coherency drop parameter sampled by the LHS technique is randomly assigned to each earthquake. To examine the impact of distance (r) on simulated ground motions, a sample of acceleration time histories simulated at three supports was selected for the case of $\alpha = 5\times10^{-4}$ sec/m: Abutment 1, Bent 4, and Bent 7 and illustrated in Fig. 8(a). The results reveal that the correlation between the simulated and the known acceleration and displacement time histories increased as the distance (r) decreased. The motion simulated at Abutment 1 was very different in terms of vibration period and amplitude. Moreover, the simulated acceleration time histories, depicted in Fig. 8(a), were converted into the respective displacement time histories, shown in Fig. 8(b), using the conversion procedure presented in Section 3. The simulated motion at Abutment 1 differed substantially from the known motion at Bent 8 with regard to both vibration period and amplitude. The

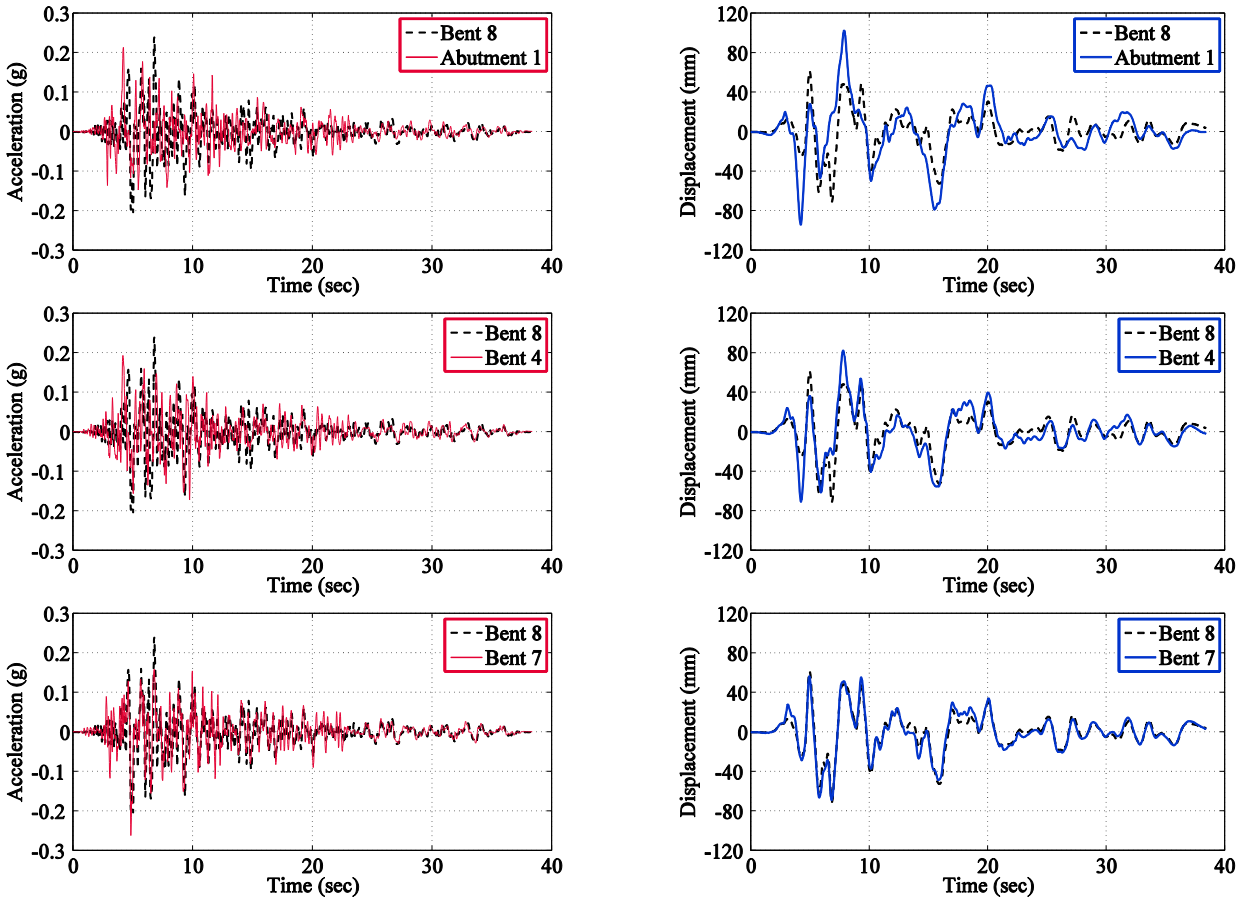

(a) Column (Bent 7) Acceleration time histories (b) Displacement time histories

Fig. 8 Simulated acceleration and displacement time histories at Abutment 1, Bent 4, and Bent 7

maximum displacement amplitude was about 1.5 times as large as the displacement amplitude of the known motion.

4.4 Probabilistic seismic demand models

Each of 100 ground motions was randomly paired with the numerical model of one of 100 bridge realizations that were generated by statistical sampling on the distribution of modeling parameters (Table 1). NTHAs for both uniform and multi-support excitations were performed for each ground motion-bridge realization pair to monitor the maximum demand (so-called engineering demand parameter (EDP)) placed on each bridge component. This study reflects the vulnerability of multiple components such as columns, superstructures, elastomeric bearings, and abutments. The EDPs used in this study were maximum column drift (θ_c in %), maximum superstructure (unseating) displacement (δ_s in mm), and maximum bearing shear strain (γ_b in %) as well as maximum passive, active, and transverse abutment displacements (δ_p, δ_a, and δ_t in mm). Moreover, this study adopted the geometric mean of two horizontal PGAs (hereafter PGA) as an intensity measure following the suggestion of the previous studies (Nielson and DesRoches 2007, Padgett and DesRoches 2008, Jeon *et al.* 2017). Here, the PGAs are the average value of PGAs recorded at all support motions for multi-support excitation analysis (Kim and Feng 2003), while they are the PGAs at the reference point for uniform excitation analysis.

Conventionally, current design practice has used uniform acceleration time histories for performing dynamic analyses. In contrast, the program OpenSees (McKenna 2011) requires displacement time histories for multi-support excitation analyses. PSDMs for EDPs were developed using the average PGA for uniform (acceleration time histories) and multi-support (displacement time histories) excitations, respectively. Comparison results of PSDMs for the bridge components under uniform and multi-support excitations are depicted in Fig. 9. Components chosen in the figure are the column drift (θ_c) at Bent 7, superstructure displacement at Hinge 13, and bearing shear strain at Hinge 3. All figures reveal that multi-support excitation analysis produced higher seismic demands for all of the selected components in that the slope and intercept of these demand models were higher than those obtained from uniform excitation analysis. Also, in the case of multi-support motions, the dispersions for the column at Bent 7, the superstructure action at Hinge 13, and the bearing at Hinge 3 are smaller than the corresponding dispersions for the uniform excitation case by 16%, 18%, and 7%, respectively.

4.5 Limit state models

As indicated before, capacity-based limit state models follow a two-parameter lognormal distribution (median and

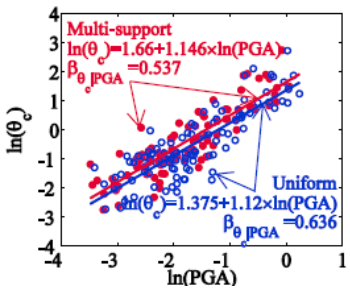

(a) Column (Bent 7)

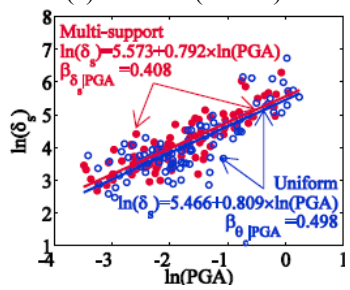

(b) Superstructure (Hinge 13)

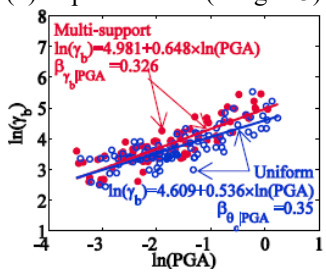

(c) Bearing (Hinge 3)

Fig. 9 Comparison of PSDMs obtained from uniform and multi-support excitation analyses

dispersion) and are presented in Table 3. To define limit state models for steel-jacketed columns, this study established the relationship of column damage and structural response (maximum drift) based on the results of 13 laboratory column tests (Chai *et al.* 1991, Sun *et al.* 1993, Priestley *et al.* 1994b, ElGawady *et al.* 2010). Column limit states were defined as maximum drifts on the onset of visible damage described in Padgett and DesRoches (2008); slight limit state was defined at the point where considerable shear cracking at the column-footing connection forms or spalling of cover concrete occurs; moderate limit state was identified as the point where permanent concrete dilatation results in jacket yielding and visual bulging on the tension side; extensive limit state was characterized as the point where unstable hysteretic response is observed and tension longitudinal rebar potentially fractures; and complete limit state is defined as the point where rapid strength degradation occurs along with potential jacket buckling and longitudinal rebar fracture. Based on visible damage descriptions, the median value and dispersion of four limit states for steel-jacketed columns are proposed in terms of maximum drift.

Avşar *et al.* (2011) proposed two limit states (damage control and collapse prevention) for superstructure displacement (unseating) for hinges at bents and abutments. The damage control limit state was defined as the case of

Table 3 Bridge component limit state models

Component		LS1 (slight)		LS2 (moderate)		LS3 (extensive)		LS4 (complete)	
		S_C	β_C	S_C	β_C	S_C	β_C	S_C	β_C
Column drift (%), θ_c		1.41	0.22	2.75	0.24	3.90	0.22	5.00	0.18
Unseating displacement (mm), δ_s	Hinges 3 and 7	–	–	–	–	762	0.47	864	0.47
	Hinges 9 and 11	–	–	–	–	508	0.47	762	0.47
	Hinge 13	–	–	–	–	559	0.47	762	0.47
Bearing shear strain (%), γ_b		100	0.60	150	0.55	200	0.59	350	0.65
Abutment displacement (mm)	Passive, δ_p	37	0.46	146	0.46	–	–	–	–
	Active, δ_a	10	0.70	38	0.90	77	0.85	–	–
	Transverse, δ_t	10	0.70	38	0.90	77	0.85	–	–

superstructure girders falling over the pedestal to rest directly on the cap beams, while the collapse prevention limit state was defined as the case of superstructure displacement exceeding an available seat width provided by the cap beams. The latter condition refers to superstructure unseating and system collapse. Thus, the limit state models for superstructure deformation (unseating) depend primarily on the dimensions of the cap beams and the abutments. By inference, this study adopted the above two limit states as extensive and complete limit states for superstructure displacement at all in-span hinges. The corresponding median values, presented in Table 3, were calculated based on available seat width at each in-span hinge. In the case of limit states with unknown dispersions, Nielson and DesRoches (2007) assumed that the COV for the higher limit states are 0.50, resulting in a dispersion of 0.47.

The limit states for elastomeric bearings were adopted as those proposed by Padgett and DesRoches (2008). The shear strain of the bearings (γ_b) was calculated as the ratio of bearing displacement to bearing height. Additionally, the limit states for abutment (passive, active, and transverse) responses followed the work of Neilson and DesRoches (2007). Moreover, the restrainer cables and deck poundings do not affect the limit states for the component capacities, although they alter the seismic demand of other components (Padgett and DesRoches 2008).

4.6 Comparison of component fragility curves using uniform and multi-support excitations

As previously indicated, with a lognormal distribution of the component capacity and demand, the component fragility curve is developed for both uniform and multi-support excitation analyses. Using the PSDMs (Fig. 9) and limit state models (Table 3), the comparison of the component fragility curves for both excitation analyses is depicted in Fig. 10. The comparison results indicate that multi-support excitation analysis increases the probability of reaching a limit state over the entire range of PGA, thereby increasing the vulnerability of the components. This finding is clearly illustrated in Fig. 11(a), which plots the difference in the median value of component fragilities obtained from both excitation analyses. This median value (λ_{PGA}) is defined as PGA at a 50% probability of observed damage state. A positive value indicates a less vulnerable

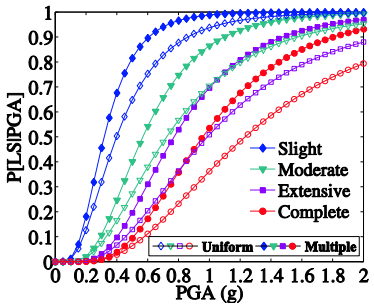

(a) Column (Bent 7)

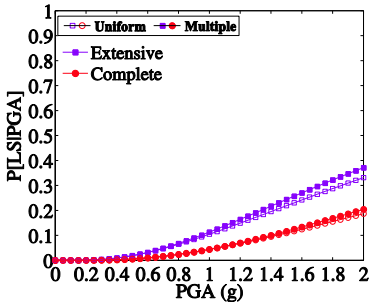

(b) Superstructure (Hinge 13)

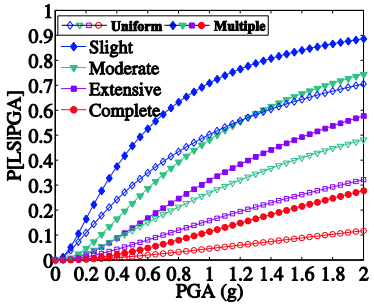

(c) Bearing (Hinge 3)

Fig. 10 Comparison of component fragility curves obtained from uniform and multi-support excitation analyses

component, while a negative value means a more vulnerable one. It was observed that all components except for one action at Abutment 17 were more vulnerable to multi-support excitations. For the columns, multi-support excitation analysis decreases the median PGA by 10~20%. In the case of the superstructures, multi-support excitation exacerbates most significantly the possibility of unseating at Hinge 3 (58% reduction) and Hinge 7 (28% reduction). However, this reduction does not indicate more vulnerable component among all components. The bearings had the same trend as the superstructures. Multi-support excitation analysis decreased the median PGA for the passive, active, and transverse actions at Abutment 1, but it increased the median PGA for the transverse action (slight limit state) at Abutment 17. In conclusion, it appears that the simulated multi-support motions increased the vulnerability of components. Moreover, the comparison of the dispersion of fragility curves (β_{PGA}) of component fragility curves obtained from the above two excitation analyses is plotted in Fig. 11(b). Multi-support excitation analysis reduced the dispersion by 10-21% for the columns, by 7-19% for the superstructures, by 1-19% for the bearings, and by 3-21% for the abutments with respect to uniform excitation

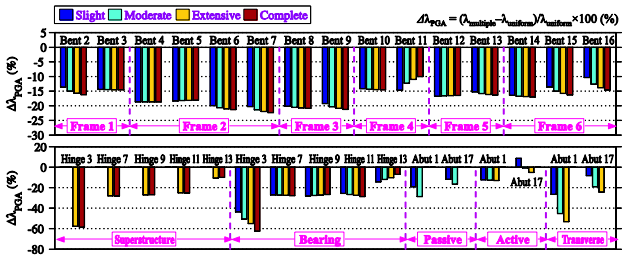

(a) Difference in the median value of fragility curves ($\Delta\lambda_{PGA}$)

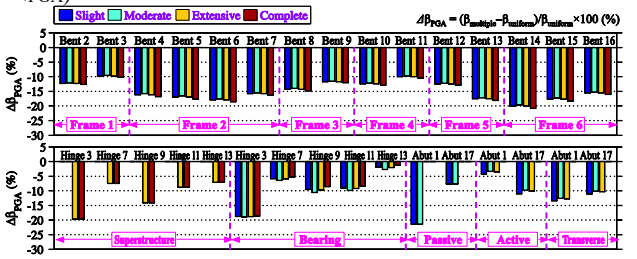

(b) Difference in the dispersion of fragility curves ($\Delta\beta_{PGA}$)

Fig. 11 Comparison of median and dispersion of component fragility curves obtained from uniform and multi-support excitation analyses

analysis. This reduction resulted from the reduced dispersion in the PSDMs as shown in Fig. 9.

5. Conclusions

This study investigated the seismic performance and fragility of a long, curved multi-frame, concrete bridge subjected to multi-support excitations. To accomplish this goal, a numerical bridge model which captures the nonlinear behavior of components was built using OpenSees. The bridge (the Northwest Connector freeway interchange in Colton, California) was struck by the 1992 Landers and Big Bear earthquakes. Especially, the numerical model of elliptical steel-jacketed columns (with partial and full height) was developed and compared with experimental results available in the literature. The validation results indicated that the simulation model provided a realistic hysteretic response in terms of stiffness, strength, and energy dissipation.

To conduct fragility assessment for the selected bridge, uncertainty models accounting for different material and structural properties were built. Then, treating an existing ground motion suite as known motions, acceleration time histories at multiple supports were simulated using a conditional stochastic random process. Then, the simulated acceleration time histories were converted into associated displacement time histories. The existing ground motion suite (acceleration time histories) was used for uniform excitation analysis and the simulated displacement time histories were used for multi-support excitation analysis in order to obtain probabilistic seismic demand models (defined as linear regression models for demand-PGA pairs) for individual components. These demand models were convolved with limit state models proposed in this study to develop component fragility curves. A comparison of the

results of component fragility curves obtained from uniform and multi-support excitation analyses indicated that the uniform excitation approach underestimates seismic demand and vulnerability for most components as compared to a more realistic approach that considers the spatial correlation of ground motions. Specifically, although multi-support excitation analysis increased the median PGA for a few components at the abutments, it reduced the median PGA for the columns by 10-20%, for the superstructures by 10-58%, and for the bearings by 7-62%. Moreover, the dispersion comparison of component fragility curves revealed that multi-support excitation analysis decreased the dispersion of component fragility curves for all components: by 10-21% for the columns, by 7-19% for the superstructures, by 1-19% for the bearings, and by 3-21% for the abutments. In conclusion, the observed results demonstrate the importance of the proper consideration of spatial variation of ground motions for long, multi-frame bridges.

Acknowledgments

The research was supported by a grant (18CTAP-C130227-02) from Technology Advancement Research Program (TARP) funded by Ministry of Land, Infrastructure and Transport of Korean government

References

Avşar, Ö., Yakut, A. and Caner, A. (2011), "Analytical fragility curves for ordinary highway bridges in Turkey", *Earthq. Spectr.*, **27**(4), 971-996.

Baker, J.W., Shahi, S.K. and Jayaram, N. (2011), *New Ground Motion Selection Procedures and Selected Motions for the PEER Transportation Research Program*, Report No. PEER Report 2011/03, Pacific Earthquake Engineering Research Center, University of California, Berkeley, CA, U.S.A.

Bos, R., De Waele, S. and Broersen, P.M.T. (2002), "Autoregressive spectral estimation by application of the Burg algorithm to irregularly sampled data", *IEEE Trans. Instr. Measure.*, **51**(6), 1289-1294.

Buckle, I.G., Friedland, I., Mander, J., Martin, G., Nutt, R. and Power, M. (2006*), Seismic Retrofitting Manual for Highway Structures: Part 1-Bridges*, Report No. MCEER-06-SP10, Multidisciplinary Center for Earthquake Research, SUNY Buffalo, NY, U.S.A.

Burg, J.P. (1972), "The relationship between maximum entropy spectra and maximum likelihood spectra", *Geophys.*, **37**(2), 375-376.

Butterworth, S. (1930), "On the theory of filter amplifiers", *Exper. Wire. Wire. Eng.*, **7**, 536-541.

Caltrans (2013), *Seismic Design Criteria (SDC) Version 1.7*, Office of Structures Design, California Department of Transportation, Sacramento, CA, U.S.A.

Caltrans (2017), *Bridge Design Aids*, California Department of Transportation, Sacramento, CA, U.S.A.

Celik, O.C. and Ellingwood, B.R. (2010), "Seismic fragilities for non-ductile reinforced concrete frames-role of aleatoric and epistemic uncertainties", *Struct. Saf.*, **32**(1), 1-12.

Choi, E., DesRoches, R. and Nielson, B. (2004), "Seismic fragility of typical bridges in moderate seismic zones", *Eng. Struct.*, **26**(2), 187-199.

Deodatis, G., Saxena, V. and Shinozuka, M. (2000), "Effect of spatial variability of ground motion on bridge fragility curves", *Proceedings of the 8th ASCE Specialty Conference on Probabilistic Mechanics and Structural Reliability*, University of Norte Dame, IN, U.S.A.

Der Kiureghian, A. (1996), "A coherency model for spatially varying ground motions", *Earthq. Eng. Struct. Dyn.*, **25**(1), 99-111.

ElGawady, M., Endeshaw, M., McLean, D. and Sack, R. (2010), "Retrofitting of rectangular columns with deficient lap splices", *J. Compos. Constr.*, **14**(1), 22-35.

Fenves, G.L. and DesRoches, R. (1994), *Response of the Northwest Connector in the Landers and Big Bear Earthquakes*, Report No. UCB/EERC-94/12: Earthquake Engineering Research Center, University of California at Berkeley, CA, U.S.A.

Haddadi, H., Shakal, A., Stephens, C., Savage, W., Huang, M., Leith, W., Parrish, J. and Borcherdt, R. (2008), "Center for engineering strong-motion data (CESMD)", *Proceedings of the 14th World Conference on Earthquake Engineering*, Beijing, China.

Hu, L., Xu, Y.L. and Zheng, Y. (2012), "Conditional simulation of spatially variable seismic ground motions based on evolutionary spectra", *Earthq. Eng. Struct. Dyn.*, **41**(15), 2125-2139.

Jackura, K.A., Beddard, D.L., Abghari, A. and Ehsan, J. (1991), *Study of Liquefaction Potential at the I-10/I-215 Interchange in San Bernardino County*, Report No. 08-Sbd-10 PM 24.19 & 24.30; E.A. 08-349304: California Department of Transportation, Sacramento, CA, U.S.A.

Jeon, J.-S., Choi, E. and Noh, M.H. (2017), "Fragility characteristics of skewed concrete bridges accounting for ground motion directionality", *Struct. Eng. Mech.*, **63**(5), 647-657.

Jeon, J.-S., DesRoches, R., Kim, T. and Choi, E. (2016), "Geometric parameters affecting seismic fragilities of curved multi-frame concrete box-girder bridges with integral abutments", *Eng. Struct.*, **122**, 121-143.

Kim, S.H. and Feng, M.Q. (2003), "Fragility analysis of bridges under ground motion with spatial variation", *J. Non-Lin. Mech.*, **38**(5), 705-721.

Konakli, K. and Der Kiureghian A. (2011), *Stochastic Dynamic Analysis of Bridges Subjected to Spatially Varying Ground Motions*, Report No. PEER 2011/105: Pacific Earthquake Engineering Research Center, University of California at Berkeley, CA, U.S.A.

Liao, S. and Zerva, A. (2006), "Physically compliant, conditionally simulated spatially variable seismic ground motions for performance-based design", *Earthq. Eng. Struct. Dyn.*, **35**(7), 891-919.

Luco, J. and Wong, H. (1986), "Response of a rigid foundation to a spatially random ground motion", *Earthq. Eng. Struct. Dyn.*, **14**(6), 891-908.

Ma, Y. and Deng, N. (2000), *Deep Foundations*, In Bridge Engineering Handbook, ed. W.F. Chen and L. Duan, CRC Press LLC, Boca Raton, FL, U.S.A.

Mander, J.B., Priestley, M.J.N. and Park, R. (1988), "Theoretical stress-strain model for confined concrete", *J. Struct. Eng.*, **114**(8), 1804-1826.

McKenna, F. (2011), "OpenSees: A framework for earthquake engineering simulation", *Comput. Sci. Eng.*, **13**(4), 58-66.

Medina, R.A. and Krawinkler, H. (2003), *Seismic Demands for Nondeteriorating Frame Structures and Their Dependence on Ground Motions*, Report No. 144: The John A. Blume Earthquake Engineering Center, Stanford University, CA, U.S.A.

Megally, S.H., Silva, P.F. and Seible, F. (2002), *Seismic Response of Sacrificial Shear Keys in Bridge Abutments*, Report No.

SSRP-2001/24: University of California at San Diego, CA, U.S.A.

Moehle, J.P. (1994), *Preliminary Report on the Seismological and Engineering Aspects of the January 17, 1994 Northridge Earthquake*, Report No. UCB/EERC-94/01: Earthquake Engineering Research Center, University of California at Berkeley, CA, U.S.A.

Muthukumar, S. and DesRoches, R. (2006), "A Hertz contact model with non-linear damping for pounding simulation", *Earthq. Eng. Struct. Dyn.*, **35**(7), 811-828.

Nielson, B.G. and DesRoches, R. (2007), "Seismic fragility methodology for highway bridges using a component level approach", *Earthq. Eng. Struct. Dyn.*, **36**(6), 823-839.

Pacific Earthquake Engineering Research Center (PEER) (2015), http://peer.berkeley.edu/nga/index.html.

Padgett, J.E. and DesRoches, R. (2008), "Methodology for the development of analytical fragility curves for retrofitted bridges", *Earthq. Eng. Struct. Dyn.*, **37**(8), 1157-1174.

Peña Ramos, C.E. and Haldar, A. (2013), "Three-dimensional response of reinforced concrete bridges under spatially varying seismic excitation", *Proceedings of the 11th International Conference on Structural Safety & Reliability (ICOSSAR)*, Columbia University, New York, U.S.A.

Priestley, M.J.N., Seible, F. and Calvi, G.M. (1996), *Seismic Design and Retrofit of Bridges*, John Wiley & Sons Inc., New York, U.S.A.

Priestley, M.J.N., Seible, F., Xiao, Y. and Verma, R. (1994a), "Steel jacket retrofitting of reinforced concrete bridge column for enhanced shear strength-part 1: Theoretical considerations and test design", *ACI Struct. J.*, **91**(4), 394-405.

Priestley, M.J.N., Seible, F., Xiao, Y. and Verma, R. (1994b), "Steel jacket retrofitting of reinforced concrete bridge column for enhanced shear strength-part 2: Test results and comparison with theory", *ACI Struct. J.*, **91**(5), 537-551.

Shafieezadeh, A., Ramanathan, K., Padgett, J.E. and DesRoches, R. (2012), "Fractional order intensity measures for probabilistic seismic demand modeling applied to highway bridges", *Earthq. Eng. Struct. Dyn.*, **41**(3), 301-409.

Shamsabadi, A., Khalili-Tehrani, P., Stewart, J.P. and Taciroglu, E. (2010), "Validated simulation models for lateral response of bridge abutments with typical backfills", *J. Brid. Eng.*, **15**(3), 302-311.

Shinozuka, M., Saxena, V. and Deodatis, G. (2000), *Effect of Spatial Variation of Ground Motion on Highway Structures*, Report No. MCEER-00-0013, Multidisciplinary Center for Earthquake Research, SUNY Buffalo, New York, U.S.A.

Somerville, P., Smith, N., Punyamurthula, S. and Sun, J. (1997), *Development of Ground Motion Time Histories for Phase 2 of the FEMA/SAC Steel Project*, Report No. SAC/BD-97/04: SAC Joint Venture, Sacramento, CA, U.S.A.

Sun, Z., Seible, F. and Priestley, M.J.N. (1993), *Flexural Retrofit of Rectangular Reinforced Concrete Bridge Columns by Steel Jacketing*, Report No. SSRP-93/01: Department of Applied Mechanics and Engineering Sciences, University of California at San Diego, CA, U.S.A.

United States Geological Survey (USGS) (2015), http://www.usgs.gov/.

Vanmarcke, E.H. and Fenton, G.A. (1991), "Conditioned simulation of local fields of earthquake ground motion", *Struct. Saf.*, **10**(1-3), 247-264.

Vanmarcke, E.H., Heredia-Zavoni, E. and Fenton, G. (1993), "Conditional simulation of spatially correlated earthquake ground motion", *J. Eng. Mech.*, **119**(11), 2333-2352.